JOURNAL OF MATERIALS SCIENCE **36** (2001) 5237–5243

Characteristics of rolling contact fatigue of steels produced by thermomechanical processing

BYUNG-YOUNG CHOI
School of Advanced Materials Engineering and Research Institute of Advanced Materials Development, Chonbuk National University, Chonju 561-756, Korea
E-mail: bychoi@moak.chonbuk.ac.kr

CHANG-SOON LEE
Division of Materials and Chemical Engineering, Sun Moon University, Asan 336-708, Korea

0.27C-1.97Cr-1.65Mn-0.30Mo-0.21Ni steels produced by thermomechanical processing were rolling contact fatigue tested in the elastohydrodynamic lubricating condition at the rotating speed of 8,000 rpm under the applied load in the range of 25–100 kgf. A mixture of lower bainite and martensite was formed during thermomechanical processing, and it was found in transmission electron microscopy that fine lower bainite was formed by splitting in two after formation of martensite. The zone of maximum shear stress was found to be 195.0–339.3 μm in depth from the contact surface by comparing the regions of hardness increase, microstructural change and the contact width during rolling contact fatigue. Resistance to crack initiation during rolling contact fatigue is the main reason for improved fatigue life. This is confirmed from the result that the shortest fatigue life was shown in the specimen with the largest crack length and crack depth.

1. Introduction

Thermomechanical processing is an advanced processing technique designed to improve the mechanical properties of materials by controlling, on-line, hot deformation processes as well as to shape the product. This process has advantages of saving energy and reducing the processing steps by eliminating heat treatment after hot deformation. It is mainly composed of plastic deformation in the austenite recrystallization region and non-recrystallization region followed by interrupted accelerated cooling. Very fine grained ferrite and martensite, bainite are formed in the thermomechanically processed steels, depending on cooling rate, and substructures of dislocations and subgrains result in high strength and toughness [1, 2]. Increased hardening through addition of substitutional elements such as Mn, Mo, Cr and Ni to the thermomechanically processed steels is achieved.

Applied load acting on the contact surface of rails, wheels and bearings during repeated rolling contact in service causes local plastic deformation and initiation and propagation of fatigue cracks resulting in flaking at surface. Higher speed operation of transportation systems and machine elements recently accelerates earlier failure of rails, wheels and bearings by rolling contact fatigue. Thus the development of materials with higher resistance to rolling contact fatigue is in need. Recent studies on bearing materials produced by high frequency induction hardening showed that rolling contact fatigue life was improved through optimization of hardening depth [3, 4]. But on-line control in manufacture has not been easy because of additional processes. Other studies revealed the high resistance to rolling contact fatigue of high strength bainitic steels [5], and local plastic deformation by repeated shear stresses just below the contact surface during rolling contact fatigue resulting in high strain hardening [6]. All these results were concerned with rolling contact fatigue of the materials after heat treatment. However, the experimental results on rolling contact fatigue of the thermomechanically processed steels without additional heat treatment has not been reported yet. It is important to understand rolling contact fatigue behaviors of the thermomechanically processed steels in order to develop materials with high resistance to rolling contact fatigue by thermomechanical processing.

In this study rolling contact fatigue testing has been conducted on materials, steels containing Mn, Mo, Cr and Ni, produced by thermomechanical processing in order to provide basic data necessary in developing materials with higher resistance to rolling contact fatigue. Characterization of microstructures, transformation of each phase and strain hardening behavior by repeated plastic deformation were discussed in terms of rolling contact fatigue life including initiation and propagation of fatigue cracks to clarify rolling contact fatigue characteristics of thermomechanically processed steels.

TABLE I Chemical composition of specimen (wt%)

C	Cr	Mn	Mo	Ni	Fe
0.27	1.97	1.65	0.30	0.21	bal.

2. Experimental procedure

2.1. Materials and thermomechanical processing

Carbon steels were melted in high frequency vacuum induction melting furnace at 1600°C with 3.0×10^{-2} Torr, followed by first charging of Cr, Ni, Mo, second charging of Mn, and third charging of C. Argon gas was inserted to control the furnace environment, and the solidified ingot was stripped in MgO crucible. The chemical composition was analyzed as shown in Table I using vacuum spectroscopy.

Ingots of 60 mm thickness were heated for 1 hr at 1200°C followed by hot rolling 11 passes before descaling. They were rolled finally to 14.7 mm thickness at 791°C, and cooled down in 3 zone cooling chamber under controlled water spraying of 3.8–4.0, 3.9 and 3.0–3.1 m^3/hr, respectively, at each cooling zone. The temperature of the product was measured to be 784°C at an entrance of cooling chamber and 493°C at an exit of cooling chamber, and the specimens were then cooled in the air after controlled cooling.

2.2. Rolling contact fatigue test

Specimens for rolling contact fatigue test were machined to the round bar with 9.525 mm diameter and 100 mm length parallel to the direction of hot rolling and the surface roughness, dimensions and straightness were measured. Rolling contact fatigue test was conducted under elastohydrodynamic lubricating conditions using Polymet RCF-1 tester as shown in Fig. 1. Lubricating oil of Shell Tellus 37 was supplied during test at a rate of 20 drops per minute at contact surface of specimen and disc. The tests were carried out at a rotating speed of 8,000 rpm under applied load of 25–100 kgf. The load applied on the specimen was measured using a strain indicator connected to the load cell. When the vibration level due to flaking reached the preset condition of the sensor, the operation was terminated and the number of rotation was recorded as the rolling contact fatigue life of the specimen.

2.3. Hardness distribution of thermomechanically processed and rolling contact fatigued specimens

Hardness of the thermomechanically processed specimens was measured repeatedly at 100 μm interval in depth from the surface using a Vickers microhardness tester under applied load of 300 g, and the hardness distribution curve was plotted and compared with that of the specimens after rolling contact fatigue test. The relationship between the comparison of hardness distribution before and after rolling contact fatigue test and fatigue life of the specimens was investigated to reveal the effect of strain hardening behavior on the rolling contact fatigue life.

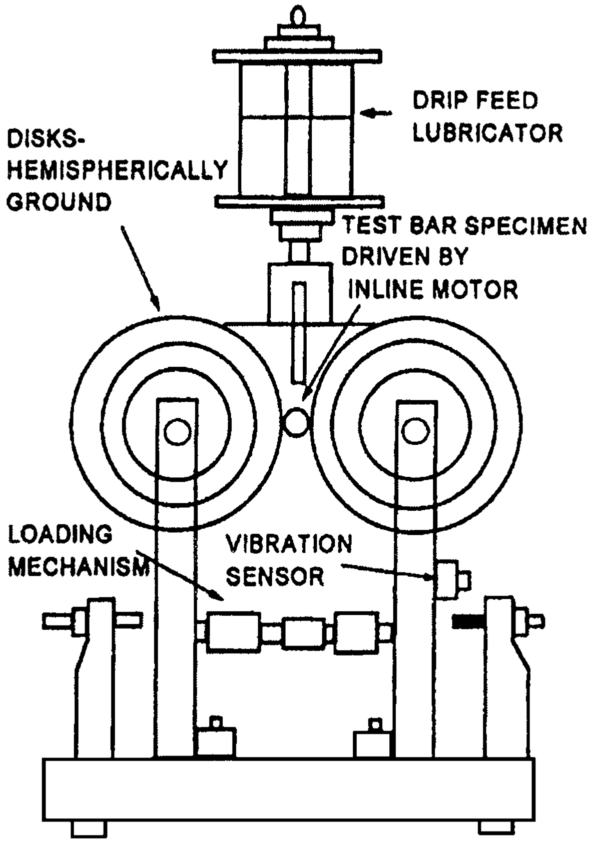

Figure 1 Schematic diagram of rolling contact fatigue tester.

2.4. Microstructural change and crack initiation and propagation during rolling contact fatigue

Microstructural change and crack initiation and propagation behavior during rolling contact fatigue were analyzed by observing the stressed region on the raceway surface. The whole area of the raceway was scanned and its cross-section was examined for precise measurement of deformed area using Taylor Hobson surface roughness tester. On the basis of the previous results the width of raceway and the depth profile were investigated and measured by computer analysis. Cross-sections of the flaked region were observed along the depth from the surface to see the microstructural change and fatigue crack initiation and propagation. The direction of crack propagation and the crack depth were analyzed to measure the degree of crack branching and deflection. The retained austenite was measured quantitatively by direct comparison method using X-ray diffractometer.

3. Results and discussion

3.1. Microstructure and hardness distribution after thermomechanical processing

Fig. 2 shows that the optical microstructure of surface area of the specimen produced by thermomechanical processing has a mixture of martensite and bainite. The microstructural change with depth from the surface showed mostly bainitic structure with some martensite structure as shown in Fig. 3. Transmission electron

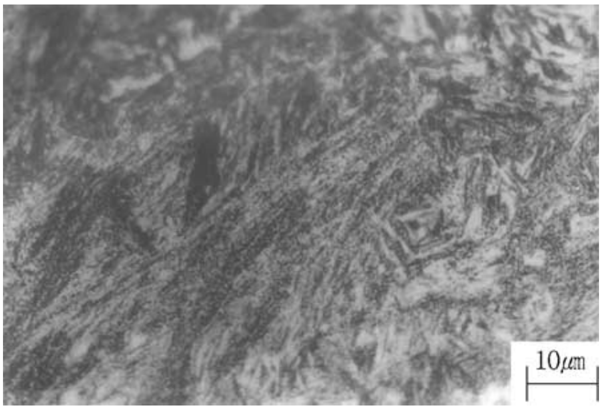

Figure 2 Optical micrograph showing martensite and bainite in the surface of thermomechanically processed steel.

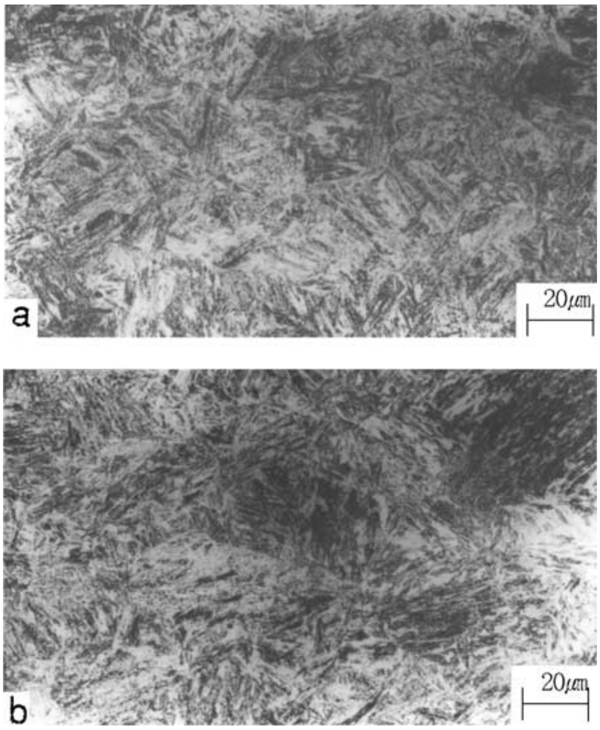

Figure 3 Optical micrographs showing mainly bainite and martensite in the subsurface of thermomechanically processed steel with depth from the surface (a) 1,000 μm (b) 3,000 μm.

micrograph revealed that the bainitic carbides were formed along a certain orientation in bainitic ferrite, and that the tangled dislocations were formed in the martensite just below the bainite, bainitic carbide also formed underneath the lath boundaries in lower region as shown in Fig. 4.

Martensite was formed at the surface region during rapid cooling of water spraying stage and lower bainite or type III bainite was formed because of difference in cooling rate along the depth from the surface and heat transfer [7–9]. Fig. 4 shows the formation of fine lower bainite through separation of lower bainite by martensite with tangled dislocations. X-ray diffraction analysis using Mo K_α radiation did not reveal the trace of retained austenite, which is thought to come from precipitation of bainitic carbides [10] caused by carbon enrichment in untransformed austenite through atomic diffusion of interstitial carbon, not reaching chemical stability of austenite [11].

Repeated measurement using a Vickers microhardness tester at 100 μm interval in depth from the surface after thermomechanical processing showed a distribution of Hv 382–445 as shown in Fig. 5. The average value was about Hv 405 in agreement with the result of homogeneous formation of a mixture of lower bainite and martensite as shown in Figs 2 and 3.

3.2. Transformation and deformation behavior during rolling contact fatigue

Fig. 6 shows the variation of hardness after repeated loading during rolling contact fatigue test. Hardness increased markedly at 200–400 μm depth from the surface, and the maximum hardness increase was shown in the specimen under 100 kgf of loading among the applied load range. When the load is applied during repeated rolling contact, shear stress is accumulated with maximum value at 200–400 μm depth, and local plastic deformation increases dislocation density causing strain hardening [12].

Fig. 7 is an S-N curve showing rolling contact fatigue life of the specimen with variation of applied load. The minimum fatigue life was shown in the specimen under 100 kgf loading, and the time to reach final failure by flaking at surface increased with decrease in applied load.

Microstructures just below the contact surface after rolling contact fatigue test are shown in Fig. 8. White etching bands were found parallel to a certain direction, and many bands were formed in a broad area under 200 μm from the contact surface in the specimen under 100 kgf as shown in Fig. 8a. On the other hand the microstructure formed during thermomechanical processing is well sustained in the specimen under 25 kgf as shown in Fig. 8b. Shear stress by repeated loading during rolling contact fatigue causes local plastic deformation, and the white etching bands were formed by stress-induced diffusion along dislocation which acted as paths for high diffusion in severely deformed ferrite region [13]. In the case of 100 kgf loading applied shear stress is high, and high dislocation density in severely deformed ferrite region makes stress-induced diffusion much easier than that of 25 kgf loading. This causes white etching bands formed in wide area of specimen under 100 kgf loading as shown in Fig. 8a and high strain hardening as shown in Fig. 6. Stress concentration occurs in these white etching bands, and crack initiation and propagation during rolling contact fatigue cause final failure and less fatigue life as shown in Fig. 7.

Taylor Hobson surface roughness measurement indicated the average roughness along the centerline was R_a 0.160–0.215, and the depth profiles of the raceway formed during rolling contact fatigue test under 100 kgf are shown in Figs 9–11. Fig. 9 is the cross-sectional profile of the whole area around the raceway, and the increased height at the right side of the raceway boundary above the specimen surface means the indentation behavior of ductile specimen by plastic deformation during rolling contact fatigue. The main portion of the raceway showed the small micropits formed

Figure 4 TEM micrograph showing bainitic carbides and martensite in the thermomechanically processed steel.

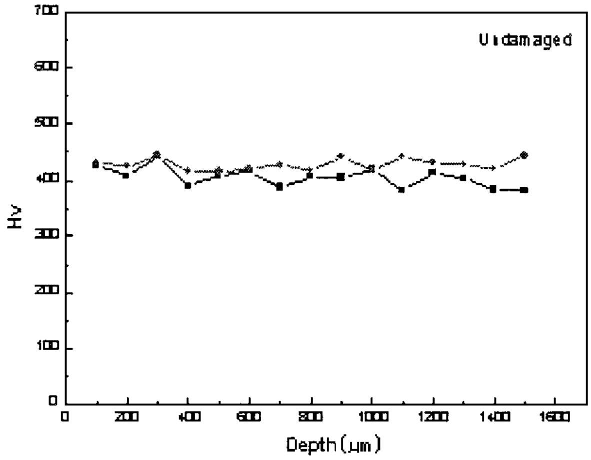

Figure 5 Microhardness variation as a function of depth from the surface in the thermomechanically processed steel.

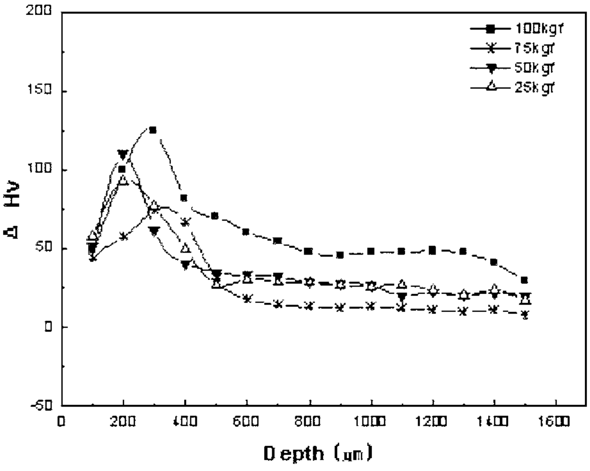

Figure 6 Variation in the microhardness increase with depth from the surface after rolling contact fatigue test.

on the cross-sectional profile, and the large micropits on the right side as shown in Fig. 10. These micropits are formed by microfailure of asperities due to asperity contact during rolling contact fatigue or many small micropits are dispersed in whole area after early plastic deformation. This causes no flaking by local failure, resulting in high resistance to rolling contact fatigue. The width of the raceway was measured to be about 870 μm as shown in Fig. 10, and Fig. 11 shows the cross-sectional profile of the flaked region with depth of about 170 μm. The thin area of disk type next to deep flaking is the raceway area and flaking occurred at the raceway center region. Analysis of the cross-sectional profile of the raceway formed in the specimens during rolling contact fatigue test under repeated loading showed that the width of the raceway decreased with decrease in the applied load, and the depth and the width of flaking were independent of applied load. The width of raceway was 501–870 μm, and the depth and the width of flaking were 51–170 μm and 323–829 μm, respectively.

According to distortion energy hypothesis and main shear stress hypothesis the applied shear stress is maximum at the depth of 0.7b–0.78b just below the

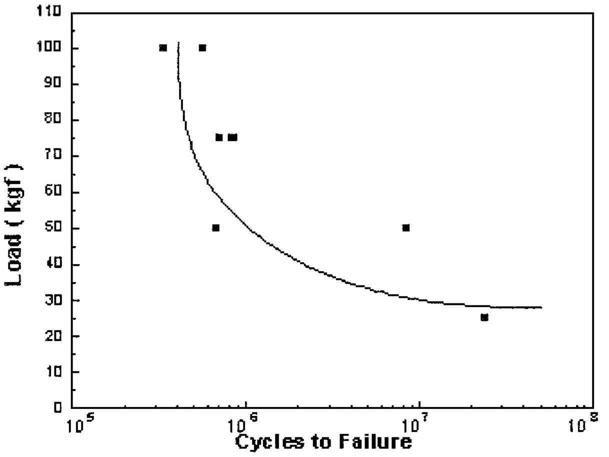

Figure 7 S-N curve showing relationship between applied load and rolling contact fatigue life.

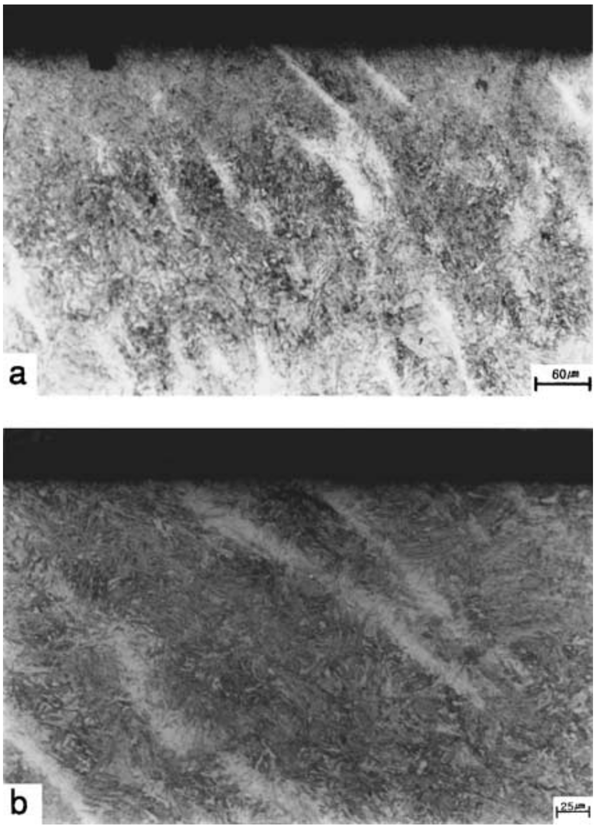

Figure 8 Optical micrographs showing microstructural change during rolling contact fatigue under applied load (a) 100 kgf and (b) 25 kgf.

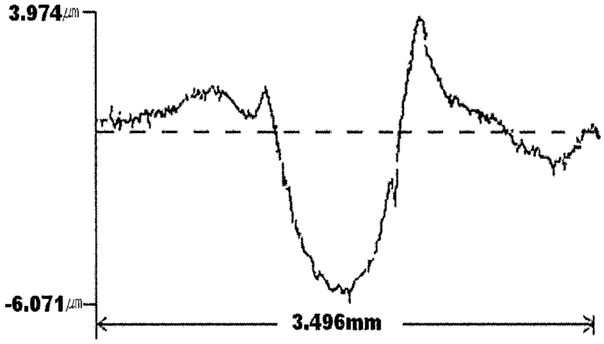

Figure 9 Cross-sectional profile of raceway after rolling contact fatigue test under applied load of 100 kgf.

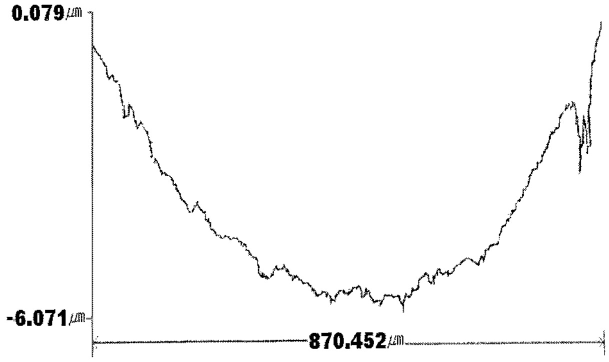

Figure 10 Cross-sectional profile of main portion of raceway after rolling contact fatigue test under applied load of 100 kgf.

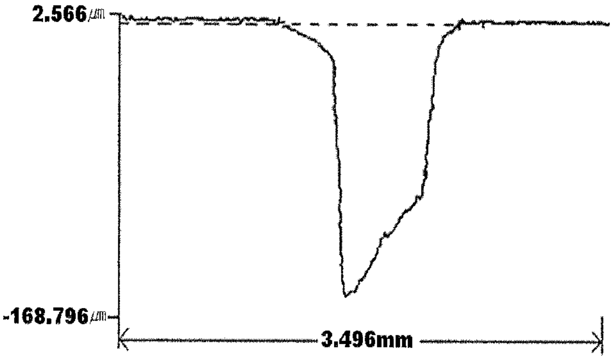

Figure 11 Cross-sectional profile of flaking in the region of raceway after rolling contact fatigue test under applied load of 100 kgf.

raceway [14] where b is the half-width of the raceway during rolling contact fatigue test under elastohydrodynamic lubricating condition. Analysis of the hardness profile (Fig. 6) and the microstructure (Fig. 8a) below the raceway revealed that $0.78b$ of 195.0–339.3 μm is very close to the measured value. The area of maximum shear stress during rolling contact fatigue test can be identified through measurement of the width of raceway after rolling contact fatigue test. Higher applied load increases the area of plastic deformation by shear stress, and the width of the raceway becomes wider, resulting in deeper region of maximum shear stressing.

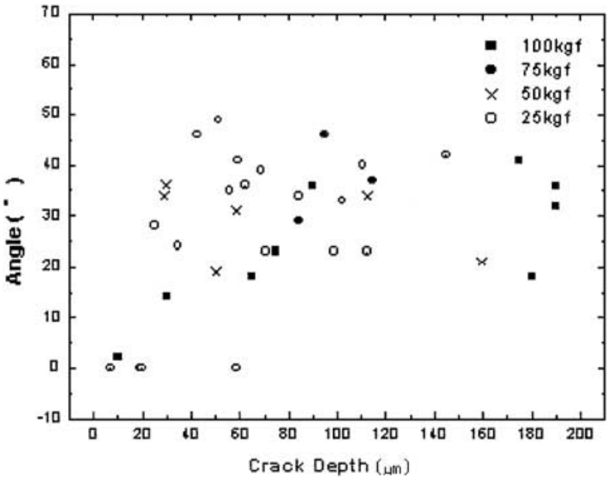

Figure 12 Relationship between crack depth and crack angle during rolling contact fatigue.

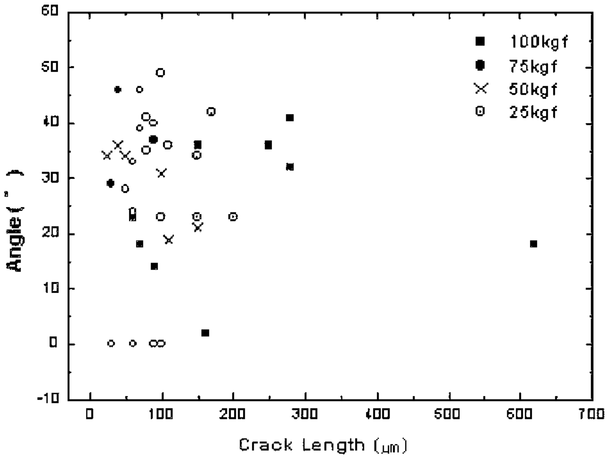

Figure 13 Relationship between crack length and crack angle during rolling contact fatigue.

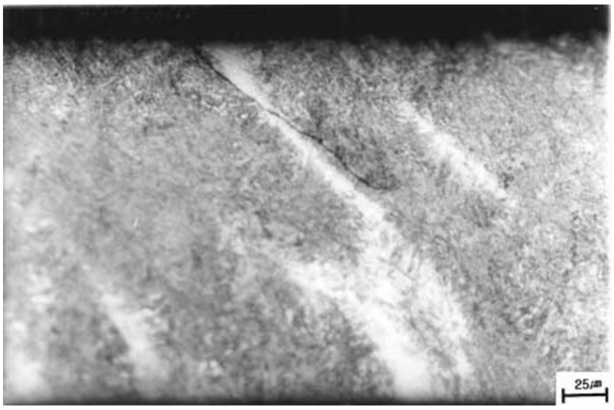

Figure 14 Optical micrograph showing subsurface crack in the rolling contact fatigue test under applied load of 100 kgf.

3.3. Crack initiation and propagation behavior during rolling contact fatigue

Depth, length and propagation angle were measured for many cracks observed depending on the applied load, and these are plotted in Figs 12 and 13. Cracks with maximum depth or maximum length were observed in the specimens subjected to loading of 100 kgf. But Fig. 7 shows these specimens have the minimum fatigue life in spite of the maximum crack length or crack depth. Rolling contact fatigue life is divided into two steps, the time needed for fatigue crack to initiate and the time for crack to propagate until flaking.

The white etching bands were formed at the region underneath the raceway by the applied load before fatigue cracks to nucleate, and many white etching bands in broad area of the specimen under 100 kgf loading were formed as shown in Fig. 8. When the additional load was applied on the white etching bands formed by severe plastic deformation, local concentration of deformation led to initiation of fatigue cracks [15]. Initiation of fatigue cracks in a specimen under 25 kgf was more difficult than that of 100 kgf, resulting in longer fatigue life because of microstructure with higher resistance to fatigue crack initiation.

Fatigue crack was observed as shown in Fig. 14 to propagate in the direction of main shear [16] along the white etching band under the raceway in a specimen under 100 kgf loading. Under the same load many cracks were formed in the white etching bands and propagated towards the surface leading to surface failure by flaking as shown in Fig. 15. Fig. 16 shows the initiation and propagation behavior of fatigue cracks observed in the specimen subjected to 50 kgf of loading, and less white etching bands were formed than that of 100 kgf of loading as shown in Figs 14 and 15. Fatigue crack length was shorter but fatigue life was longer than those under 100 kgf of loading as shown in Fig. 7, which indicates

Figure 16 Optical micrograph showing subsurface cracks to flaking in the rolling contact fatigue test under applied load of 50 kgf.

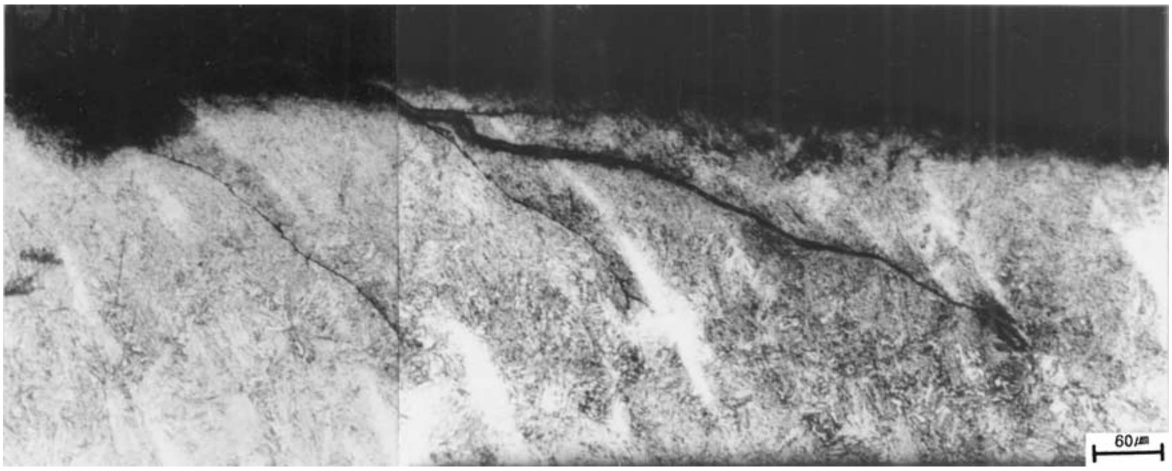

Figure 15 Optical micrograph showing subsurface cracks to flaking in the rolling contact fatigue test under applied load of 100 kgf.

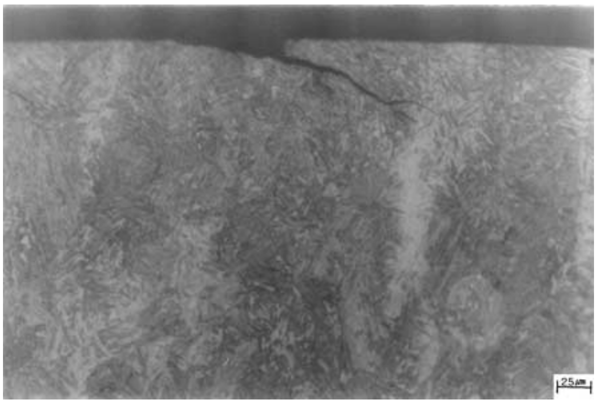

Figure 17 Optical micrograph showing subsurface cracks to flaking in the rolling contact fatigue test under applied load of 25 kgf.

higher resistance to fatigue crack initiation resulting in longer fatigue life. Fig. 17 shows the fatigue cracks observed at the region just below the raceway when the specimen was subjected to 25 kgf of loading. Crack length was short, but caused flaking at the surface, and the longest fatigue life was due to the highest resistance to crack initiation.

4. Conclusions

0.27C-1.97Cr-1.65Mn-0.30Mo-0.21Ni steels produced by thermomechanical processing were rolling contact fatigue tested in the elastohydrodynamic lubricating condition at the rotating speed of 8,000 rpm under the applied load range of 25–100 kgf. The following conclusions were obtained from this study.

1. A mixture of lower bainite and martensite was formed during thermomechanical processing, and TEM study showed the fine lower bainite was formed by splitting in two after formation of martensite.

2. The region of maximum shear stress was measured to be 195.0–339.3 μm in depth from the surface of the raceway by comparing the regions of hardness increase and the microstructural change during rolling contact fatigue.

3. Resistance to crack initiation during rolling contact fatigue is the main reason for improved fatigue life. This is confirmed from the results that the shortest fatigue life was shown in the specimen with the largest crack length and crack depth.

Acknowledgment

The authors wish to acknowledge the financial support of the Korea Research Foundation made in the program year of 1998.

References

1. Y. SAITO, *ISIJ* (1989) 187.
2. O. V. MISHIN *et al., Scripta Met.* **35** (1996) 873.
3. B. Y. CHOI *et al., Wear* **192** (1996) 1.
4. B. Y. CHOI, in Proceedings of 6th International IFHT, 1997, p. 283.
5. D. X. XU and G. X. LU, *Wear* **169** (1993) 153.
6. Y. G. LEE and B.Y. CHOI, *Kor. J. Metals* **31**(4) (1993) 500.
7. A. Z. SAHIN, B. S. YILBAS and A. Z. AL-GARNI, *Int. Comm. Heat Mass Transfer* **21**(2) (1994) 199.
8. Y. OHMORI, *Jap. J. Metals* **29**(7) (1990) 542.
9. H. K. D. H. BHADESHIA and J. W. CHRISTIAN, *Metall. Trans. A* **21A** (1990) 767.
10. B. Y. CHOI, G. KRAUSS and D. K. MATLOCK, *Scripta. Met.* **22**(9) (1988) 1575.
11. K. TSUZAKI and T. MAKI, *J. Japan Soc. Heat Treatment* **32**(1) (1992) 10.
12. B. Y. CHOI and G. W. BAHNG, *Mat. Sci. Tech.* **14** (1998) 816.
13. D. A. PORTER and K. E. EASTERLING, in "Phase Transformations in Metals and Alloys" (Van Nostrand Reinhold, 1981) p. 102.
14. H. SCHLICHT *et al., Ball and Roller Bearing Engineering* **1** (1987) 14.
15. B. Y. CHOI and J. S. JANG, *Kor. J. Mat.* **8**(12) (1998) 1176.
16. V. BHARGAVA, G.T. HAHN and C. A. RUBIN, *Wear* **133** (1989) 65.

Received 20 July 2000
and accepted 24 April 2001